The possible effects of including ridge-related roughness in air-ice drag parameterization: a sensitivity study

L.-B. Tremblay and L.A. Mysak

Department of Atmospheric and Oceanic Sciences

and

Centre for Climate and Global Change Research

McGill University, 805 Sherbrooke St. West, Montreal, Quebec Canada, H3A 2K6.

The effects of including ridge-related roughness in the drag parameterization on the ice thickness distribution is investigated using a sea-ice dynamic and thermodynamic model. A long-term integration of the sea ice model forced by the 5-day running mean of daily geostrophic winds and steady but spatially varying ocean currents was performed to construct climatological thickness fields. Compared to the case of a constant drag coefficient, the results including the roughness have a significantly different spatial distribution with much thicker ice in the western Arctic; this is in better agreement with observations.

1 Introduction

The presence of sea ice in the polar regions has a substantial influence on the global climate. In particular, the sea ice acts as an insulator, reducing the amount of ocean heat lost to the atmosphere. In turn, the ability of ice to insulate is a strong function of its thickness. Since the ice thickness distribution can be altered by the opening of leads, in regions of divergence, or ridging, in regions of convergence, ice dynamics should be properly included in climate model studies of the Arctic.

Of the terms in the ice momentum equation, most of the uncertainty lies in the formulation of the internal ice stress term and in the wind and ocean forcing on the pack ice. A lot of attention has been placed (and still is) on the proper modelling of the internal ice stress term (rheology) which involves the derivation of constitutive relations that try to capture

the important features of sea-ice deformation under applied load (Hibler, 1979; Flato and Hibler, 1992; Tremblay and Mysak, 1997). In this note, however, we will concentrate on the wind and ocean forcing terms. In most previous studies (Hibler, 1979; Flemming and Semtner, 1991; Flato and Hibler, 1992; Holland *et al.*, 1993), a square drag law with constant drag coefficient is used to model the air-ice and ice-water stresses. However, more recent measurements have demonstrated that the wind drag coefficient can vary widely depending on the ice surface roughness and presumably, also on the atmosphere stratification (Smith, 1990). Anderson (1987) also found large variations in the measured drag coefficient in the ice-edge region which depended on the ice concentration. In the present study, the effects of including ridging-related surface roughness in the air-ice and water-ice drag parameterization is presented.

In section 2, a brief description of the model used for this simulation is given, and in section 3, supporting evidence for using a variable drag coefficient for modelling studies in the Arctic is presented. In section 4, the sea ice thickness winter climatology obtained from a 10-year integration for both constant and roughness-dependent drag coefficients are compared with submarine sonar data. The main conclusions drawn from the simulation results are summarized in the last section.

2 Model description

The sea-ice model is forced with prescribed atmospheric temperatures, winds and ocean currents. In the ice momentum equation, the acceleration term is neglected, i.e., the ice is assumed to be in balance with the external forcing. For this reason, a 5-day running mean of the daily varying winds are used. The constitutive relations used in this model are derived assuming the ice behaves as a large-scale granular material with no cohesion (Tremblay and Mysak, 1997). In particular, ice is considered to have no resistance to tensile forces, a fixed resistance to a compressive load which is a function of ice thickness, and shear resistance proportional to the local internal ice pressure. A single-layer thermodynamic model with a

linear internal temperature profile is used for the sea ice. The surface energy flux between the ice-ocean surface and the atmosphere includes latent and sensible heat components, as well as shortwave and longwave radiation. In the present model the ocean is allowed to warm up even though ice is present in a grid cell. The transfer of heat between the ocean and the ice is achieved through sensible heating in a similar manner as between the ice and the atmosphere. A detailed description of the model is given in Tremblay and Mysak (1997).

3 Drag law parameterization

The drag coefficients can be calculated from direct stress measurements (u'w') or from wind measurements assuming a specific structure of the planetary boundary layer. The air-ice and ocean-ice stresses are usually modelled as a quadratic law with constant turning angle (McPhee, 1975) as follows:

$$\begin{aligned} \boldsymbol{\tau}_a &= \rho_a C_{da} |\boldsymbol{u}_a^g| \ (\boldsymbol{u}_a^g \cos\theta_a + \boldsymbol{k} \times \boldsymbol{u}_a^g \sin\theta_a), \\ \boldsymbol{\tau}_w &= \rho_w C_{dw} |\boldsymbol{u}_i - \boldsymbol{u}_w^g| \ \left[(\boldsymbol{u}_i - \boldsymbol{u}_w^g)\cos\theta_w + \boldsymbol{k} \times (\boldsymbol{u}_i - \boldsymbol{u}_w^g)\sin\theta_w\right], \end{aligned}$$

in which ρ_a and ρ_w are the air and water densities, C_{da} and C_{dw} the air and water drag coefficients, $\boldsymbol{u}_a^g$ and $\boldsymbol{u}_w^g$ the geostrophic wind and ocean current, $\boldsymbol{u}_i$ the ice velocity, θ_a and θ_w the wind and water turning angles and $\boldsymbol{k}$ a unit vector normal to the surface. Typical values for C_{da} and C_{dw} are 1.2×10^{-3} and 5.5×10^{-3}, respectively. In the above equation for the wind shear stress, the ice speed is considered small compared to the wind speed and is therefore neglected.

For the atmospheric case, various measurements made over the last 30 years yield drag coefficients ranging from 1 to 6×10^{-3}, with more recent measurements being higher (figure 1). However, in most sea ice modelling studies, a lower-range C_{da} value of 1.2×10^{-3} is used instead (Hibler, 1979; Flato and Hibler, 1992; Holland *et al.*, 1993) . This choice is based on boundary layer measurements made during the AIDJEX project in 1972 (figure 1). The

increasing trend with time in the measured drag coefficients is due to the measurements being made over increasingly rough surfaces and perhaps under increasingly unstable stratification conditions (Smith, 1990).

In this study, we attempt to include the effect of surface roughness in the drag parameterization; however, we ignore the influence of atmospheric stratification. To zeroth order, we assume that sea ice surface roughness is determined by the ridging intensity. Since ridging results in the buildup of thicker ice, the sea ice surface roughness is assumed to depend on the ice thickness. Stössel and Claussen (1993) have also, among other factors, considered a dependence of the form drag on the ice-plus-snow freeboard. The relation between ice thickness and ridging intensity in the Arctic can be seen by comparing the observed ridging frequency distribution (figure 2) with the measured ice thickness distribution in the Arctic (figure 3-c). For the water-ice drag coefficient, the same dependence on surface roughness is assumed.

The lower range of measured drag coefficients (around 1×10^{-3}) commonly used in large-scale sea ice modelling studies are assumed characteristic of one-meter thick ice; the larger range values (around 5×10^{-3}) are assumed to apply to 5-meter thick ice (see figure 1). Inside those bounds, the drag coefficients are assumed to vary linearly with ice thickness; outside those bounds, the drag coefficients are specified to have these minimum or maximum values. Mathematically, this parameterization can be written as follows:

$$C_{da,w} = C'_{da,w} \begin{cases} 1m, & \mathrm{h} < 1\mathrm{m} \\ h, & 1\mathrm{m} < \mathrm{h} < 5\mathrm{m} \\ 5m, & \mathrm{h} > 5\mathrm{m}, \end{cases}$$

in which h is the sea ice thickness and, C'_{da} and C'_{dw} the base drag coefficients taken as 1×10^{-3} and 5.5×10^{-3}, respectively. The linear dependence of C_{dw} on ice thickness h also allows the momentum and continuity equations to be written in terms of the ice flux $\boldsymbol{u}_i h$, which permits the use of more correct boundary conditions (i.e., no normal flux of ice at a solid boundary).

4 Results

Results from a 10-year simulation of the sea-ice cover in the Arctic Ocean and surrounding seas are presented in this section. A cartesian mesh with a grid resolution of 111 km is used on a polar stereographic projection of the physical domain. At high latitudes, the variation of the Coriolis parameter with latitude is small and the f-plane approximation is used. The model is forced with the prescribed 1961 5-day running mean of the daily geostrophic winds with its yearly mean replaced by the 1954-89 annual climatology obtained from the NMC sea level pressure analysis (Flato and Hibler, 1992). This provides winds representative of climatology with realistic weekly variability. There is no particular reason for choosing the year 1961 except that it was not an anomalous year in term of sea ice circulation, as were 1969 and 1984, for example. Spatially varying, but steady ocean currents were calculated from a single layer reduced gravity model, appropriate for large scale flows, where the acceleration term in the momentum equation is ignored, friction is represented using a linear drag law, and the normal velocity component is specified at open boundaries. In the Bering Strait, the normal velocity was set to obtain a constant inflow of 1 SV into the Arctic. The inflow and outflow velocity field in the North Atlantic was specified from Levitus sea surface elevation data and scaled in such a way as to obtain no accumulation of water in the Arctic domain. Finally, the solar forcing is the daily average value corrected for an 80 % cloud cover (Laevastu, 1960).

The boundary conditions for the ice dynamic equations are zero normal and tangential velocity at a solid boundary and free outflow at an open boundary (Hibler, 1979). For the sea ice thermodynamic equation, the atmospheric temperature is specified from monthly climatology. The temperature at a given day is calculated as a weighted average of the mid-month climatological values. These temperatures were calculated from the NMC 850 mb height and temperature fields, assuming a linear temperature profile between the 1013 mb and 850 mb levels. For the ocean, the temperatures at open boundaries are specified from monthly climatologies extracted from the Levitus data. At continental boundaries, the ocean heat flux is considered zero (a continent is regarded as a perfect insulator).

The model was integrated for 10 years to reach a stable seasonal cycle using a 1-day time step. To isolate the effects of the drag law parameterization on the simulated thickness distribution fields, the same ocean currents and atmospheric temperature fields are used in the simulations. The results shown are the simulated winter climatological thickness distributions using a constant and a thickness dependent drag coefficient. The model results are compared with sonar data for ice thickness.

4.1 March ice thickness and ice edge position

Figure 3-a shows the simulated winter climatological thickness distributions in the Arctic using a constant drag coefficient, which can be compared with the sonar measurements (figure 3-c) reported by Bourke and Garrett (1987). The ice edge position, defined as the 5-tenth ice concentration contour, is also included in these figures. The model contour line patterns reproduce the observations reasonably well, with ice thickness ranging from 1 meter near the Asian continent, to 7 meters north of Greenland. In the Laptev and East Siberian seas, the simulated ice thickness (2-3 m) is larger than observed ($<$ 1m). The modelled ice free region in the North Atlantic extends over the whole Norwegian and Barents seas due to the advection of warm water by the Norwegian Current. In the winter, whether the Bering Strait is open or closed has a strong influence on the ice thickness distribution in the Chukchi Sea. When open, the resulting ocean current pattern produces significantly thicker ice north of the Bering Strait. However, the temperature of the water entering the domain is very close to freezing point and thus does not have a significant influence on the growth of ice in this region. In the Barents Sea, the ice margin is very well reproduced; however, in the Greenland Sea the ice edge is too far east. This is due to the prescribed ocean currents which have a weak recirculation of water in the Greenland Sea.

Figure 3-b shows the simulated mid-March thickness distribution in the Arctic using a roughness dependent drag coefficient as described in the previous section. In this simulation, the ice thickness also ranges from 1 to 7 meters, as before. However, now the ice thickness spatial distribution poleward of the northern Canadian Islands is significantly different and

is in better agreement with the observations. In this region, the ridging activity is high and the ice is assumed rough; this results not only in a higher wind stress but also in ice drift following the wind more closely (ratio of water drag to Coriolis effect is higher). Both of these effects contribute to a higher ice buildup against the western part of the northern Canadian coast, as observed in the thickness field (figure 3-c). In thinner ice regions the roughness-dependent drag coefficients approach the minimum value and little difference in the thickness distribution is found for the two models.

5 Conclusions

In the present study, ice surface roughness is assumed to increase with ridging intensity, which in turn is responsible for ice thickening. Consequently, the drag coefficients are considered proportional to ice thickness. The effects of the atmospheric stability on the air-ice momentum transfer, however, is not considered.

A long term integration of the sea ice model with both a constant and roughness dependent drag coefficient yield a range in ice thickness in good agreement with ice observations. However, the ice thickness spatial distribution in the Canada Bassin for the two simulations is significantly different. The results using a constant drag coefficient yield a more uniform thickness buildup against the northern Canadian islands whereas, the results using the roughness dependent drag coefficient results in an offshore tongue of thicker ice in the western Arctic; this is in better agreement with the thickness observations. In general, the simulations show that spatially varying drag coefficients, within the range of observed values, have a strong influence on the calculated ice thickness distribution, and an attempt to incorporate this effect into sea ice modelling studies is desirable.

6 Acknowledgment

Bruno Tremblay is grateful to NSERC and FCAR, and Prof. L.A. Mysak to AES and NSERC for their financial support during the course of this work.

References

Anderson, R. J. (1987). Wind stress measurements over rough ice during the 1984 marginal ice zone experiment. *Journal of Geophysical Research*, 92:6933–6941.

Bourke, R. H. and Garrett, R. P. (1987). Sea ice thickness distribution in the Arctic Ocean. *Cold Regions Science and Technology*, 13:259–280.

Flato, G. M. and Hibler, III, W. D. (1992). Modeling pack ice as a cavitating fluid. *Journal of Physical Oceanography*, 22:626–651.

Flemming, G. H. and Semtner, A. J. (1991). A numerical study of interannual ocean forcing on Arctic sea ice. *Journal of Geophysical Research*, 96:4589–4603.

Hibler, III, W. D. (1979). A dynamic thermodynamic sea ice model. *Journal of Physical Oceanography*, 9:815–846.

Holland, D. M., Mysak, L. A., and Manak, D. K. (1993). Sensitivity study of a dynamic-thermodynamic sea-ice model. *Journal of Geophysical Research*, 98:2561–2586.

Laevastu, T. (1960). Factors affecting the temperature of the surface layer of the sea. *Commentationes physico-mathematicae*, 25(1).

McPhee, M. G. (1975). Ice-ocean momentum transfer for the aidjex ice model. *AIDJEX Bulletin*, 29:93–111.

Smith, W. O. (1990). *Polar Oceanography. Part A: Physical Science*. Academic Press.

Stössel, A. and Claussen, M. (1993). On the momentum forcing of a large-scale sea-ice model. *Climate Dynamics*, 9:71–80.

Tremblay, L.-B. and Mysak, L. A. (1997). Modelling sea ice as a granular material, including the dilatancy effect. *accepted by Journal of Physical Oceanography.*

Tucker, W. B. and Westhall, V. H. (1973). Arctic sea ice frequency distribution derived from laser profiles. *AIDJEX Bulletin*, 21:171–180.

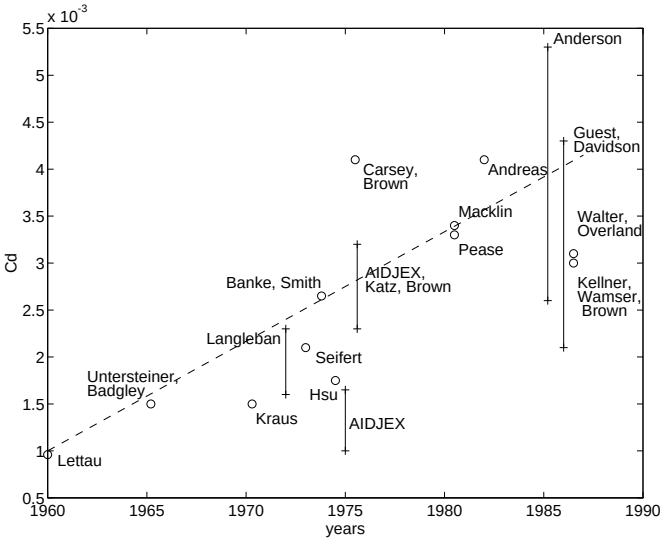

Figure 1: Drag coefficients over ice from various experiments, reproduced from Smith (1990)

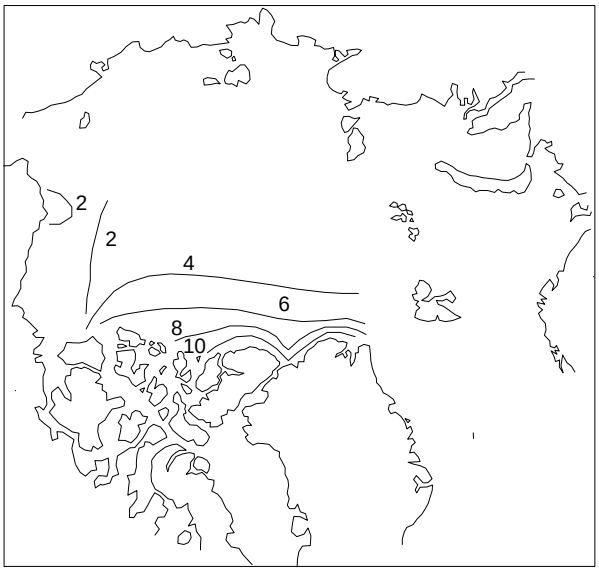

Figure 2: Number of ridges (larger than 1.22 m) per kilometer in winter, reproduced from Tucker and Westhall (1973)

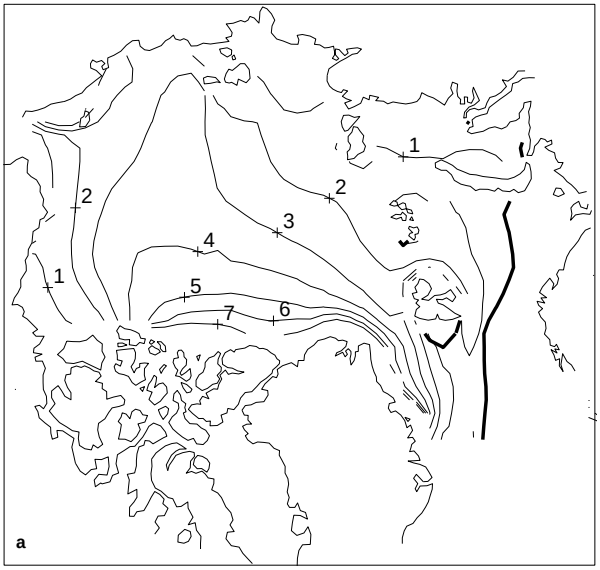

Figure 3: Simulated March ice thickness distribution with constant (a) and roughness dependent (b) drag coefficient, and observed ice thickness from sonar data (c), in meters. In (a) and (b), the ice edge is shown as a broad black line.

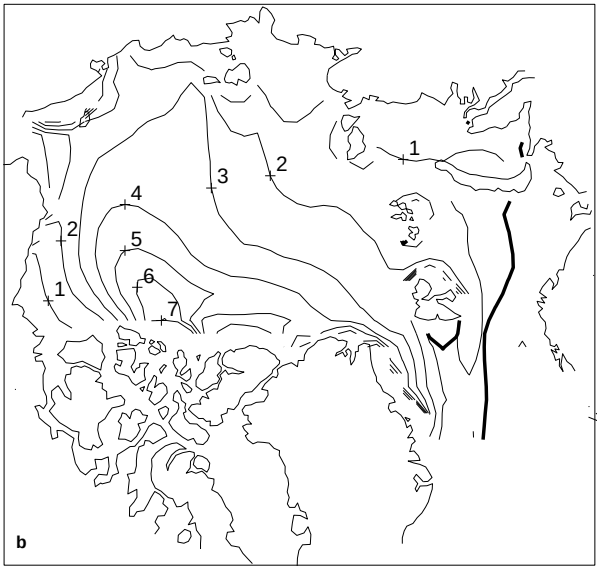

Figure 3: Simulated March ice thickness distribution with constant (a) and roughness dependent (b) drag coefficient, and observed ice thickness from sonar data (c), in meters. In (a) and (b), the ice edge is shown as a broad black line.

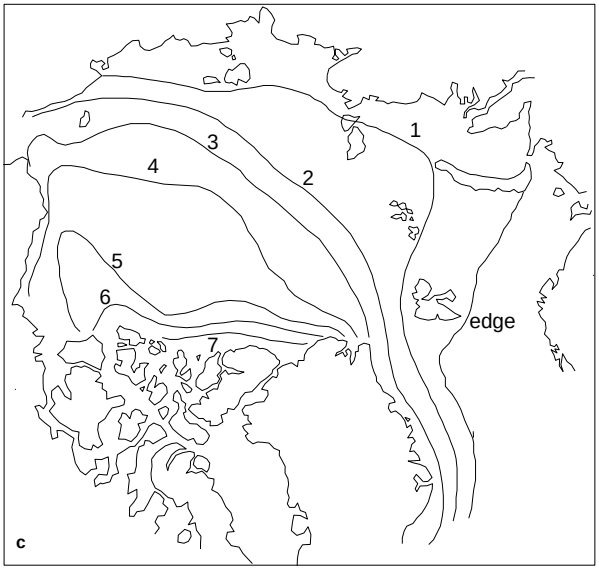

Figure 3: Simulated March ice thickness distribution with constant (a) and roughness dependent (b) drag coefficient, and observed ice thickness from sonar data (c), in meters. In (a) and (b), the ice edge is shown as a broad black line.

Figure 1: Drag coefficients over ice from various experiments, reproduced from Smith (1990)

Figure 2: Number of ridges (larger than 1.22 m) per kilometer in winter, reproduced from Tucker and Westhall (1973)

Figure 3: Simulated March ice thickness distribution with constant (a) and roughness dependent (b) drag coefficient, and observed ice thickness from sonar data (c), in meters. In (a) and (b), the ice edge is shown as a broad black line.